Theory of a curved planar waveguide with Robin boundary conditions

O. Olendski
Atomic and Molecular Engineering Laboratory, Belarusian State University, Skarina Avenue 4, Minsk 220050, Belarus

L. Mikhailovska
Department of Higher Mathematics, Military Academy, Minsk 220057, Belarus

(Received 26 June 2009; revised manuscript received 16 January 2010; published 23 March 2010)

A model of a thin straight strip with a uniformly curved section and with boundary requirements zeroing at the edges a linear superposition of the wave function and its normal derivative (Robin boundary condition) is analyzed theoretically within the framework of the linear Schrödinger equation and is applied to the study of the processes in the bent magnetic multilayers, superconducting films and metallic ferrite-filled waveguides. In particular, subband thresholds of the straight and curved parts of the film are calculated and analyzed as a function of the Robin parameter $1/\Lambda$, with Λ being an extrapolation length entering Robin boundary condition. For the arbitrary Robin coefficients which are equal on the opposite interfaces of the strip and for all bend parameters the lowest-mode energy of the continuously curved duct is always smaller than its straight counterpart. Accordingly, the bound state below the fundamental propagation threshold of the straight arms always exists as a result of the bend. In terms of the superconductivity language it means an increased critical temperature of the curved film compared to its straight counterpart. Localized-level dependence on the parameters of the curve is investigated with its energy decreasing with increasing bend angle and decreasing bend radius. Conditions of the bound-state existence for the different Robin parameters on the opposite edges are analyzed too; in particular, it is shown that the bound state below the first transverse threshold of the straight arm always exists if the inner extrapolation length is not larger than the outer one. In the opposite case there is a range of the bend parameters where the curved film cannot trap the wave and form the localized mode; for example, for the fixed bend radius the bound state emerges from the continuum at some nonzero bend angle that depends on the difference of the two lengths Λ at the opposite interfaces. Various transport properties of the film such as interference blockade of the current flow at some special energies is also discussed with the special attention being paid to the transformation from the Dirichlet to the Neumann case as the extrapolation length Λ sweeps the positive axis.

DOI: 10.1103/PhysRevE.81.036606 PACS number(s): 41.20.Jb, 74.20.De, 74.78.−w, 73.63.Nm

I. INTRODUCTION

Properties of domains confined by the surfaces $\mathcal{L}$ supporting boundary conditions involving a linear combination of both a solution $\Psi(\mathbf{r})$ of the Helmholtz wave equation

$$\Delta\Psi(\mathbf{r}) = \varepsilon\Psi(\mathbf{r}) \tag{1}$$

and its spatial derivative have been under intense research for some time. Such requirements are commonly referred to as Robin boundary condition [1] with its most general form written as

$$\mathbf{n}\,\nabla\,\Psi|_{\mathcal{L}} = \frac{1}{\Lambda}\Psi|_{\mathcal{L}}, \tag{2}$$

$\mathbf{n}$ being an inward unit vector normal to the confining interface. Robin parameter $1/\Lambda$ is, in general, a function of the two- (2D) or three-dimensional (3D) radius-vector, $\Lambda \equiv \Lambda(\mathbf{r})$. Equation (2) contains as limiting cases a Dirichlet condition of zero wave function $\Psi=0$ at $\Lambda=0$ and the Neumann requirement of vanishing its normal derivative $\partial\Psi/\partial n$ at $\Lambda=\pm\infty$. Significance of the study of such configurations is of not only pure theoretical interest [2] but also of large practical applications since this type of the boundary conditions emerges naturally in various classical and quantum structures of physics and chemistry. For example, from phenomenological theory of superconductivity [3] it is known that behavior of the order parameter $\Psi(\mathbf{r})$ near the transition point is well described by the linearized Ginsburg-Landau (GL) equation [4,5]

$$-\frac{\hbar^2}{2m}\nabla^2\Psi(\mathbf{r}) = -\alpha\Psi(\mathbf{r}). \tag{3}$$

Here, $-\alpha=[\hbar^2/2m\xi^2(0)](1-T/T_c)$ is the GL parameter with T being the actual temperature of the superconducting material, T_c being the bulk critical temperature at zero magnetic field and $\xi(0)$ representing zero-temperature coherence length. Comparing Eq. (3) with the usual Schrödinger equation [6], one sees their complete analogy; namely, Eq. (3) describes the wave function $\Psi(\mathbf{r})$ of the quantum particle of the negative charge $-2e$ (with e being the absolute value of the electronic charge) and mass m moving with a total energy

$$E \equiv -\alpha = \frac{\hbar^2}{2m\xi^2(0)}\left(1-\frac{T}{T_c}\right). \tag{4}$$

Equation (3) is supplemented for the spatially confined samples by the Robin boundary condition of the form from Eq. (2) [4,7]. In this case, the coefficient Λ is called the extrapolation length (or de Gennes distance). Analysis of the microscopic equations of superconductivity [8] leads to the expression of Λ via the parameters used in the phenomenological GL theory [9,10] with its infinite value [11] corre-

sponding physically to the interface between the superconductor and vacuum or the insulator while its positive finite magnitude describes the processes at the superconductor/normal metal surface. For superconductor/ferromagnetic boundary the extrapolation length can take vanishingly small values which means a suppression of superconductivity. Negative lengths correspond to the border with the superconductor with the higher critical temperature which physically means enhancement of the surface superconductivity. This theoretically predicted enhancement [12–14] was indeed observed in cold worked $In_{0.993}Bi_{0.007}$ foils [12] and tin samples [15]. It was estimated that in the former case the extrapolation length is $\Lambda \sim -1$ μm [13]. Negative extrapolation length appears also in the theory of twinning plane superconductivity [16]. In addition, it was argued that for the strong electric field $\mathcal{E}$ applied perpendicularly to the interface, the inverse extrapolation length $1/\Lambda$ in Eq. (2) should be supplemented (for zero magnetic field) by the term $\mathcal{E}/U_s$, where the effective potential U_s is expressed via the usual parameters of the GL theory [17]. For finding the transition temperature T from Eq. (4), one needs to find the lowest eigenvalue E_{min} of Eq. (3) with the order parameter $\Psi(\mathbf{r})$ satisfying Eq. (2). Then, it follows from Eq. (4) that

$$T = T_c\left[1 - E_{min}\frac{2m\xi^2(0)}{\hbar^2}\right]. \tag{5}$$

Accordingly, the task of minimizing E_{min} as much as possible is an actual problem of the superconductivity research leading to higher critical temperatures T.

Continuing analysis by mathematicians and physicists of the singly or multiply connected 2D or 3D regions with different boundary conditions *bounded* by one or several (piecewise) smooth curves or surfaces [2,18–26] (so called *closed* quantum billiards) entered recently into a new phase with the actively developing investigation of the *open* billiards, first of all, planar quantum waveguides. For example, properties of the straight channels with combined Dirichlet and Neumann requirements [27–34] or with the sinusoidal [35] or abrupt [36] change of the Robin parameter on one or both confining walls were calculated and, among other spectral and scattering features, an influence of this modulation on the critical temperature of the superconducting film was studied. A simplified version of the GL model of superconductivity in straight films with Robin boundary condition was derived in the asymptotic limit of very small thickness [37]. Influence of the extrapolation length on the nucleation of superconductivity in thin films in perpendicular magnetic field was calculated [38]. A comparative analysis of two straight parallel waveguides with common Dirichlet or Neumann inner boundary with one or several coupling windows and Dirichlet requirements at the outer walls was performed [39]. Such a model of distribution of boundary conditions might describe the transport and localization properties in magnetic multilayers. Even more exciting is a research of the *bent* ducts with different boundary conditions. However, before describing the fascinating features of such requirements, we found it didactically and methodologically relevant to review first the uniform boundary conditions imposed on the confining interfaces of the bent channels. We start from stating that the model of the bent waveguide with uniform Dirichlet or Neumann demand is used in many branches of physics and chemistry: its obvious application in acoustics [40,41], electrodynamics and optics [42–44], quantum theory [45,46] is also extended into such seemingly unexpected areas as elementary particle physics [47], chemical physics [48], and quantum chemistry [49]. After of almost a century of scrutinization, preceded by hints which stopped short to make finishing strokes [50–52], the most important so far discovery took place: it was predicted that a bend in the curved waveguide of constant width d with Dirichlet boundary conditions traps a charged quantum particle with its energy being smaller than the fundamental propagation threshold $\pi^2\hbar^2/(2md^2)$ of the straight arm [53–55]. Extra space in the bend presents a shelter where the charged particles can dwell with their momenta smaller than the cutoff momentum of the lowest subband. In fact, the bend creates in the straight channel an effective negative (i.e., attractive) potential with its depth and spatial extent being determined by the bend parameters [56]. Interference of the discrete level split off by the bend from the higher lying subband, with the continuum states of the lower mode, also drastically modifies the transport properties of the waveguide leading to a steep dip with zero minimum on the conductance versus energy dependence [57–59]. Experimental confirmation of the bound-state existence followed soon [60]. For the Neumann waveguide the fundamental propagation threshold is zero and no any state is split off below it by the bend. The discovery spurred an intensive research of the properties of the bent channels where we want to mark out the prediction of the existence of bound states in continuum [61] at some critical parameters of the bend [59] and an analysis of magnetic field influence on the bound states and resonances with its summary provided in Ref. [62].

As a natural extension of the research described in the previous paragraph, calculations of the bent waveguide with uniform Dirichlet and Neumann requirements on the opposite walls were performed [63–65]. In addition to the superconducting films and magnetic multilayers [39], such a model is applicable to the study of the continental shelf waves on a curved coast [66]. It was shown that such curved waveguide recurs properties of its pure Dirichlet counterpart if the inner surface supports Dirichlet condition and the outer interface obeys the Neumann requirement. Only for such configuration a bound state below the first transversal mode exists [63–66] and the steep dips to zero in the conductance-energy dependence are observed with their half widths turning to zero at some critical parameters of the bend what manifests again a formation of bound state in the continuum [64]. No bound state is split off nor any antiresonances are observed if the Dirichlet (Neumann) boundary condition is imposed on "locally longer (shorter)" boundary. Magnetic field influence on the Dirichlet inner—Neumann outer channel is also very similar to the pure Dirichlet case [67]. Thus, a very close analogy is established between Dirichlet (Neumann) inner—Neumann (Dirichlet) outer ducts and pure Dirichlet (Neumann) waveguides. Transport properties of the two waveguides of different curvatures with the external Dirichlet and inner Neumann interfaces coupled via a small window, were also calculated [68].

Recently, the research on the curved 2D strip of constant width with at least one of the interfaces supporting Robin boundary condition was promulgated [69]. With the opposite wall supporting the Dirichlet requirement, it was proved for certain Robin parameters that the estimation from below of the spectral threshold of such channel is determined by the lowest Laplacian eigenvalue of the Robin-Dirichlet annulus which, in turn, depends on the geometry of the waveguide. It was argued that after the replacement of the Dirichlet condition by the Robin one, the problem of evaluation from below of the fundamental propagation mode reduces to the study of properties of the first eigenvalue in a Robin-Robin annulus.

In the present research, we derive and analyze solutions of the Helmholtz equation, Eq. (1), with Robin boundary conditions, Eq. (2), in the 2D open domain in the form of a curved planar waveguide. In general, different constant extrapolation lengths Λ_{out} and Λ_{in} are supported by the outer and inner interfaces, respectively. As stated above, this model describes nucleation processes in thin curved superconducting films. It can also be used for studying spectral and transport properties of the magnetic multilayers; namely, it was shown before [67] that, under some relation between band gaps and widths of the two adjacent quantum wells mimicking the potential profile for the majority- or minority-spin electrons in the ferromagnetic superlattice, their properties are very well approximated by one quantum wire with the Dirichlet and Neumann boundary conditions on the opposite interfaces. However, if the above mentioned correlation between potentials and widths does not hold, one is forced to employ more general Robin boundary conditions with the extrapolation lengths chosen in such a way that satisfies all the necessary requirements. Apparently, the same boundary conditions are possible for the electromagnetic waveguides filled with ferrite [70–72]. In the present analysis, we confine our discussion to the case of *real* extrapolation lengths postponing the consideration of *complex* Λ to the future research. The last situation arises, for example, in lined acoustical ducts [73–77] where the Robin parameter is proportional to the *complex* specific acoustical admittance. It is shown in the next sections that the bound state below the fundamental propagation threshold of a straight arm always exists if the Robin coefficient is the same on the opposite confining walls, and its dependence on the extrapolation length and bend parameters is calculated. It is discovered that the curved section binds the wave inside it for all bend parameters if the outer surface is more "Neumannian" than the inner one, i.e., when the inequality $\Lambda_{out} \geq \Lambda_{in}$ holds. In the opposite regime the bound state can exist when the bend perturbation of the straight channel is sufficiently strong to bind the particle; for example, at the fixed bend radius it exists not for all bend angles as in the previous case but emerges from the continuum at some nonzero one that is a growing function of the ratio $\Lambda_{in}/\Lambda_{out}$. Transformation of the scattering characteristics from the Dirichlet to Neumann case with the positive extrapolation length growing is also discussed as well as the transmission at the negative Λ.

The paper is organized as follows. In Sec. II our model is presented and a necessary formulation of our method is given. Section III is devoted to the presentation and detailed physical interpretation of the calculated results. Summary of the research is provided in Sec. IV.

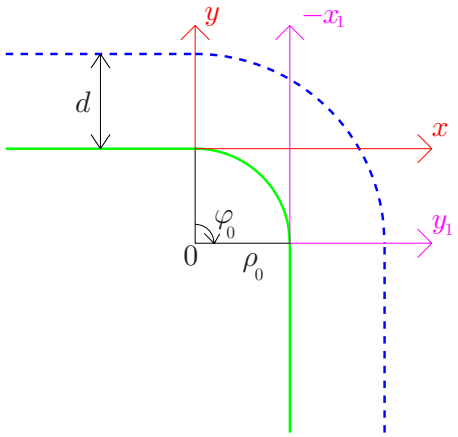

FIG. 1. (Color online) Schematic of the curved magnetic or superconducting film. The waveguide width is d and the bend angle and inner radius are φ_0 and ρ_0, respectively. The inner (thick solid line) and outer (dashed line) surfaces of the duct support uniform Robin boundary conditions with the parameters Λ_{in} and Λ_{out}, respectively, that might be different on the opposite walls. The origin of the polar coordinate system (ρ,φ) coincides with the center of the bend. The polar axis is a vertical junction of the straight and curved parts. The curved arrow shows direction in which the azimuthal angle φ grows. The local Cartesian coordinate systems (x,y) and (x_1,y_1) for the straight arms are also shown.

II. MODEL AND FORMULATION

The structure we consider is shown schematically in Fig. 1. Infinitely long strip of constant width d contains a uniformly curved section with the inner radius ρ_0 and angle φ_0. On each of the film sides we impose a uniform Robin boundary condition, Eq. (2), with, in general, different inner, Λ_{in}, and outer, Λ_{out}, extrapolation lengths. We will look for the solution of Eq. (3) in terms of the energy E, which is more relevant for the ferromagnetic channel, switching, if necessary, to the temperature T of the superconductor, according to Eqs. (4) and (5). Accordingly, we will interchangeably use both ferromagnetic as well as superconducting terms and the results will be equally applicable to both these materials, if not explicitly stated otherwise. Transition to the frequency ω of the electromagnetic waveguide is also straightforward. In our present treatment there is no magnetic field applied to the structure, however, similar to the pure Dirichlet [59,62] or Dirichlet-Neumann [64,67] cases, it can be included at the later stage. We will measure all distances in units of waveguide width d, energies—in units of the ground-state energy of infinitely deep purely Dirichlet quantum well $\pi^2\hbar^2/(2md^2)$, all momenta in units of $\hbar/d$, time—in units of $2md^2/(\pi^2\hbar)$, conductance—in units of q^2/h, where $q=e$ for the ferromagnetic layer and $q=2e$ for the superconductor.

In each part of the waveguide, a corresponding solution of Eq. (3) can be expressed in the analytical form. For example, in the straight arm to the left of the bend, a solution to Eq. (3) is

$$\Psi(x,y) = \sum_{n=1}^{\infty} (A_n e^{ik_n x} + B_n e^{-ik_n x})\chi_n(y). \tag{6}$$

First sum in Eq. (6) describes the waves incident on the bend with the wave vector k_n, with a second term being a set of

reflected (for the real k_n) or localized near it (for the imaginary k_n) modes. Complex amplitudes A_n and B_n define the relative contribution of the nth subband into the total current. In the same way, a solution after the bend reads

$$\Psi(x_1,y_1) = \sum_{n=1}^{\infty} C_n e^{ik_{\pi}x_1}\chi_n(y_1). \tag{7}$$

Again, the terms in Eq. (7) with real k_n describe the waves propagating away from the curved scatterer while the terms with imaginary momenta are the states trapped by the bend.

The boundary condition, Eq. (2), reads for the transverse function $\chi_n(y)$,

$$\left[\chi_n'(y) - \frac{1}{\Lambda_{in}}\chi_n(y)\right]\Bigg|_{y=0} = 0 \tag{8a}$$

$$\left[\chi_n'(y) + \frac{1}{\Lambda_{out}}\chi_n(y)\right]\Bigg|_{y=1} = 0. \tag{8b}$$

Equations (8) for each energy E define the wave vectors k_n according to

$$\left(1 + \frac{\Lambda_{in}}{\Lambda_{out}}\right)\cos\,\kappa_n + \left(\frac{1}{\kappa_n\Lambda_{out}} - \kappa_n\Lambda_{in}\right)\sin\,\kappa_n = 0, \tag{9}$$

$\kappa_n = \sqrt{\pi^2 E - k_n^2}$. Wave vector spectrum incorporates a finite number of real and an infinite countable set of imaginary k_n. Putting k_n equal to zero allows one to find the propagation thresholds E_{TH} of the straight waveguide with Robin boundary conditions,

$$\left(1 + \frac{\Lambda_{in}}{\Lambda_{out}}\right)\cos\,\pi\sqrt{E_{TH}} + \left(\frac{1}{\pi\sqrt{E_{TH}}\Lambda_{out}} - \pi\sqrt{E_{TH}}\Lambda_{in}\right)\sin\,\pi\sqrt{E_{TH}} = 0. \tag{10}$$

It is immediately seen from Eq. (10) that the straight duct with at least one negative extrapolation length $\Lambda_{in,out}$ supports modes with the negative energies. For example, a complete set of solutions to Eq. (10) for the equal in magnitude but opposite in sign lengths, $\Lambda_{in} = -\Lambda_{out}$, is

$$E_{TH} = -1/(\pi^2\Lambda_{in}^2), \quad n^2, n = 1,2,\ldots. \tag{11}$$

Superficially, this spectrum is very similar to the Dirichlet case except the additional negative term that makes the whole picture completely different; namely, as it follows from Eq. (5), critical temperature is substantially higher for this configuration.

Figure 2 shows propagation thresholds for the equal extrapolation lengths $\Lambda_{in} = \Lambda_{out} \equiv \Lambda$, as a function of Λ (cf. Fig. 12 of Ref. [78]). For the large magnitudes of the negative length Λ the thresholds approach those of the Neumann duct, $E_{TH}|_{\Lambda\to-\infty} = (n-1)^2$. With decreasing the magnitude of the extrapolation length, the subband boundaries with $n \geq 3$ decrease too and at the vanishing Λ they transform into those for the Dirichlet case, $E_{TH}|_{\Lambda=0} = (n-2)^2$, $n \geq 3$. Further length

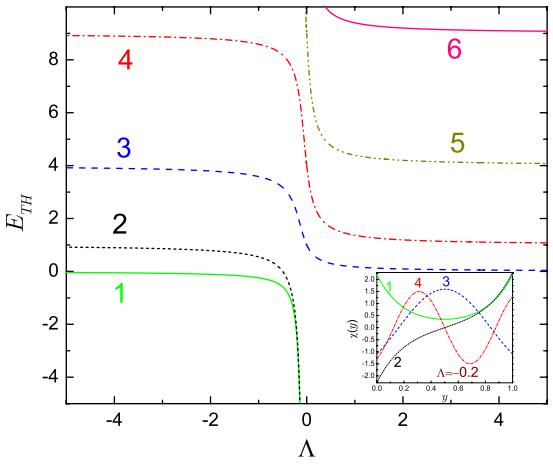

FIG. 2. (Color online) Propagation thresholds E_{TH} [solutions of Eq. (10)] in the straight waveguide as a function of the extrapolation length $\Lambda = \Lambda_{in} = \Lambda_{out}$. Numbers near the curves count thresholds in the order of increasing energy. The inset shows corresponding transverse functions $\chi(y)$ for the two negative-energy thresholds and the two lowest positive-energy states at $\Lambda = -0.2$.

growth toward the large positive values causes the thresholds to change again into the Neumann ones being, however, shifted by the two subbands compared to those at $\Lambda = -\infty$, $E_{TH}|_{\Lambda\to+\infty} = (n-3)^2$, $n \geq 3$. Completely different behavior is observed for the two lowest at $\Lambda = -\infty$ energies which decrease with $|\Lambda|$ growing and, as the extrapolation length approaches zero, these thresholds come closer and closer to each other moving simultaneously to the unrestrictedly large negative values. Such a behavior of these two split-off levels which do not have their counterparts at the positive lengths is a peculiar feature of the waveguides with *negative* Robin parameters. The number of *two* is due to the fact that the channel is confined by the *two* parallel surfaces. We address this issue in more detail while discussing the curved section. Also, it can be shown from Eq. (10) that the energy of the second level turns to zero at

$$\Lambda_{in} + \Lambda_{out} + 1 = 0 \tag{12}$$

and, thus, for the symmetric case shown in Fig. 2, at $\Lambda \leq -1/2$ the whole fundamental propagation subband lies in the negative-energy range.

The transverse function χ_n from Eqs. (6) and (7) satisfying the equation

$$\chi_n''(y) + \kappa_n^2\chi_n(y) = 0 \tag{13}$$

with the boundary conditions, Eqs. (8), is written as

$$\chi_n(y) = \sqrt{\frac{2}{1+\kappa_n^2\Lambda_{in}^2+\Lambda_{in}+(-1+\kappa_n^2\Lambda_{in}^2)\dfrac{\sin 2\kappa_n}{2\kappa_n}-\Lambda_{in}\cos 2\kappa_n}}\,(\sin\kappa_n y+\kappa_n\Lambda_{in}\cos\kappa_n y),\quad \pi^2E-k_n^2>0, \tag{14a}$$

$$\chi_n(y) = \sqrt{\frac{2}{-1+|\kappa_n|^2\Lambda_{in}^2-\Lambda_{in}+(1+|\kappa_n|^2\Lambda_{in}^2)\dfrac{\sinh 2|\kappa_n|}{2|\kappa_n|}+\Lambda_{in}\cosh 2|\kappa_n|}}\,(\sinh|\kappa_n|y+|\kappa_n|\Lambda_{in}\cosh|\kappa_n|y),\quad \pi^2E-k_n^2<0, \tag{14b}$$

$$\chi_n(y) = \sqrt{\frac{1}{\Lambda_{in}^2+\Lambda_{in}+1/3}}(y+\Lambda_{in}),\quad \pi^2E-k_n^2=0, \tag{14c}$$

with the linear dependence from Eq. (14c) existing only when, in addition to the condition $\kappa_n=0$, Eq. (12) is also satisfied.

The functions $\chi_n(y)$ of the first several subband energies are shown in the inset of Fig. 2 for the quite small negative length $\Lambda=-0.2$. It is seen that the split-off levels are located mainly at the surfaces contrary to the positive-energy levels which are spread inside the film. In other words, the negative extrapolation length in Eq. (2) attracts the particle to the corresponding interface transforming it into the surface state or, in the superconductivity terms, since the outer medium has higher critical temperature, nucleation of the superconducting state starts near the film boundaries. According to the general rules of wave mechanics [6], each nth function has $(n-1)$ nodes and for n odd (even) is symmetric (antisymmetric) with respect to the middle of the channel.

Inside the bend, in the polar coordinate system with the polar point coinciding with the center of the bend and the polar axis being the vertical junction between the straight and bent parts of the waveguide, solution of the Schrödinger equation reads:

$$\Psi(\rho,\varphi)=\sum_{n=1}^{\infty}(D_n e^{i\nu_n\varphi}+F_n e^{-i\nu_n\varphi})R_{\nu_n}(\rho) \tag{15}$$

with $R_{\nu_n}(\rho)$ being a radial part of the wave function that satisfies the Bessel differential equation

$$R''_{\nu_n}(\rho)+\frac{1}{\rho}R'_{\nu_n}(\rho)+\left(\pi^2E-\frac{\nu_n^2}{\rho^2}\right)R_{\nu_n}(\rho)=0 \tag{16}$$

supplemented by the boundary conditions,

$$\left[R'_{\nu_n}(\rho)-\frac{1}{\Lambda_{in}}R_{\nu_n}(\rho)\right]\Bigg|_{\rho=\rho_0}=0, \tag{17a}$$

$$\left[R'_{\nu_n}(\rho)+\frac{1}{\Lambda_{out}}R_{\nu_n}(\rho)\right]\Bigg|_{\rho=\rho_0+1}=0. \tag{17b}$$

Its explicit form is written as

$$R_{\nu_n}(\rho)=Q_n\Bigg\{\left[\pi\sqrt{E}Y'_{\nu_n}(\pi\sqrt{E}\rho_0)-\frac{1}{\Lambda_{in}}Y_{\nu_n}(\pi\sqrt{E}\rho_0)\right]J_{\nu_n}(\pi\sqrt{E}\rho)-\left[\pi\sqrt{E}J'_{\nu_n}(\pi\sqrt{E}\rho_0)-\frac{1}{\Lambda_{in}}J_{\nu_n}(\pi\sqrt{E}\rho_0)\right]Y_{\nu_n}(\pi\sqrt{E}\rho)\Bigg\},\quad E>0 \tag{18a}$$

$$R_{\nu_n}(\rho)=Q_n\Bigg\{\left[\pi\sqrt{|E|}K'_{\nu_n}(\pi\sqrt{|E|}\rho_0)-\frac{1}{\Lambda_{in}}K_{\nu_n}(\pi\sqrt{|E|}\rho_0)\right]I_{\nu_n}(\pi\sqrt{|E|}\rho)-\left[\pi\sqrt{|E|}I'_{\nu_n}(\pi\sqrt{|E|}\rho_0)-\frac{1}{\Lambda_{in}}I_{\nu_n}(\pi\sqrt{|E|}\rho_0)\right]K_{\nu_n}(\pi\sqrt{|E|}\rho)\Bigg\},\quad E<0. \tag{18b}$$

Here $J_\nu(\rho)$ and $Y_\nu(\rho)$ [$I_\nu(\rho)$ and $K_\nu(\rho)$] are [modified] Bessel functions of the first and second kind, respectively [79]. Coefficients Q_n are determined from the orthonormalization condition [80,81]

$$\int_{\rho_0}^{\rho_0+1}R_{\nu_n}(\rho)R_{\nu_{n'}}(\rho)d\rho/\rho=\delta_{nn'}, \tag{19}$$

$\delta_{nn'}$ is a Kronecker symbol. The first Robin requirement, Eq. (17a), is automatically satisfied by the radial function from Eqs. (18). Applying the second Robin demand, Eq. (17b), one arrives at the transcendental equation for the calculation of the angular wave vectors ν_n at the fixed energy E,

$$\left[\pi\sqrt{E}Y'_{\nu_n}(\pi\sqrt{E}\rho_0)-\frac{1}{\Lambda_{in}}Y_{\nu_n}(\pi\sqrt{E}\rho_0)\right]\times\left[\pi\sqrt{E}J'_{\nu_n}(\pi\sqrt{E}(\rho_0+1))+\frac{1}{\Lambda_{out}}J_{\nu_n}(\pi\sqrt{E}(\rho_0+1))\right]-\left[\pi\sqrt{E}J'_{\nu_n}(\pi\sqrt{E}\rho_0)-\frac{1}{\Lambda_{in}}J_{\nu_n}(\pi\sqrt{E}\rho_0)\right]$$

$$\times\left\{\pi\sqrt{E}Y'_{\nu_n}[\pi\sqrt{E}(\rho_0+1)]+\frac{1}{\Lambda_{out}}Y_{\nu_n}[\pi\sqrt{E}(\rho_0+1)]\right\}$$
$$=0, \tag{20a}$$

$$\left[\pi\sqrt{|E|}K'_{\nu_n}(\pi\sqrt{|E|}\rho_0)-\frac{1}{\Lambda_{in}}K_{\nu_n}(\pi\sqrt{|E|}\rho_0)\right]$$
$$\times\left[\pi\sqrt{|E|}I'_{\nu_n}(\pi\sqrt{|E|}(\rho_0+1))+\frac{1}{\Lambda_{out}}I_{\nu_n}(\pi\sqrt{|E|}(\rho_0+1))\right]$$
$$-\left[\pi\sqrt{|E|}I'_{\nu_n}(\pi\sqrt{|E|}\rho_0)-\frac{1}{\Lambda_{in}}I_{\nu_n}(\pi\sqrt{|E|}\rho_0)\right]$$
$$\times\left\{\pi\sqrt{|E|}K'_{\nu_n}[\pi\sqrt{|E|}(\rho_0+1)]\right.$$
$$\left.+\frac{1}{\Lambda_{out}}K_{\nu_n}[\pi\sqrt{|E|}(\rho_0+1)]\right\}=0, \tag{20b}$$

for the positive and negative energies, respectively. As mentioned before, formally the same as Eq. (20a) transcendental expression governs sound propagation in a curved duct with nonzero wall acoustic admittances [73–77] where, however, the coefficients $1/\Lambda_{in,out}$ take complex values. In the present research we deal with the real Robin parameters, so, the case of complex extrapolation lengths is not addressed below. Since the geometry of the bent film does not possess a circular symmetry, the coefficients ν_n are not real integers. Similar to the pure Dirichlet [59], Neumann [40,41] or Dirichlet-Neumann [64] curved channels, it can be shown [42,82] that the solutions of Eqs. (19) are discrete and countably infinite with only a finite number of real solutions and infinitely many imaginary ν_n. Real zeros are naturally associated with the modes propagating inside the bend, and imaginary values describe the evanescent waves.

Putting in Eqs. (19) the value of ν equal to zero allows one to find the propagation thresholds E_{TH} in the continuously curved film,

$$\left[\pi\sqrt{E_{TH}}Y_1(\pi\sqrt{E_{TH}}\rho_0)+\frac{1}{\Lambda_{in}}Y_0(\pi\sqrt{E_{TH}}\rho_0)\right]$$
$$\times\left[\pi\sqrt{E_{TH}}J_1(\pi\sqrt{E_{TH}}(\rho_0+1))\right.$$
$$\left.-\frac{1}{\Lambda_{out}}J_0(\pi\sqrt{E_{TH}}(\rho_0+1))\right]$$
$$-\left[\pi\sqrt{E_{TH}}J_1(\pi\sqrt{E_{TH}}\rho_0)+\frac{1}{\Lambda_{in}}J_0(\pi\sqrt{E_{TH}}\rho_0)\right]$$
$$\times\left\{\pi\sqrt{E_{TH}}Y_1[\pi\sqrt{E_{TH}}(\rho_0+1)]\right.$$
$$\left.-\frac{1}{\Lambda_{out}}Y_0[\pi\sqrt{E_{TH}}(\rho_0+1)]\right\}=0, \tag{21a}$$

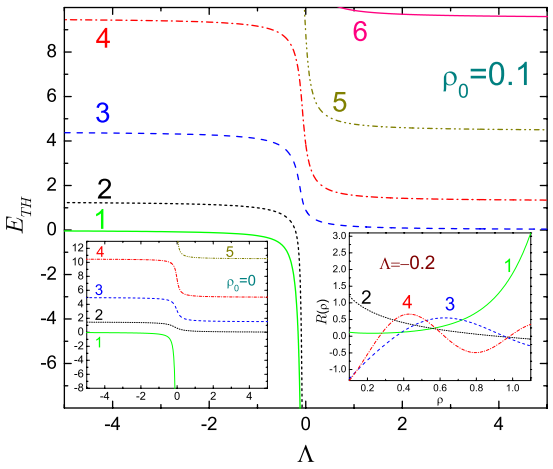

FIG. 3. (Color online) Propagation thresholds E_{TH} [solutions of Eqs. (21)] of a continuously curved waveguide with ρ_0=0.1 as a function of the extrapolation length Λ. The same convention as in Fig. 2 is used. Right inset shows corresponding radial functions $R(\rho)$ for the two negative-energy thresholds and the two lowest positive-energy levels at Λ=−0.2 while the left inset depicts thresholds for the case of zero inner radius.

$$\left[\pi\sqrt{|E_{TH}|}K_1(\pi\sqrt{|E_{TH}|}\rho_0)+\frac{1}{\Lambda_{in}}K_0(\pi\sqrt{|E_{TH}|}\rho_0)\right]$$
$$\times\left[\pi\sqrt{|E_{TH}|}I_1(\pi\sqrt{|E_{TH}|}(\rho_0+1))\right.$$
$$\left.+\frac{1}{\Lambda_{out}}I_0(\pi\sqrt{|E_{TH}|}(\rho_0+1))\right]$$
$$+\left[-\pi\sqrt{|E_{TH}|}I_1(\pi\sqrt{|E_{TH}|}\rho_0)+\frac{1}{\Lambda_{in}}I_0(\pi\sqrt{|E_{TH}|}\rho_0)\right]$$
$$\times\left\{\pi\sqrt{|E_{TH}|}K_1[\pi\sqrt{|E_{TH}|}(\rho_0+1)]\right.$$
$$\left.-\frac{1}{\Lambda_{out}}K_0[\pi\sqrt{|E_{TH}|}(\rho_0+1)]\right\}=0. \tag{21b}$$

As before, Eqs. (21a) and (21b) are written for the positive and negative energies, respectively. Note that at $\rho_0\to\infty$ Eq. (21a) transforms into Eq. (10), as expected. Similarly, Eqs. (18) and (20a) in the same limit turn into Eqs. (13) and (9), respectively.

Figure 3 depicts propagation thresholds of a continuously curved film with the bend radius ρ_0=0.1 as a function of the extrapolation length Λ. Qualitatively, the overall picture is the same as for the straight duct; namely, with Λ growing from the large negative values to zero all the levels but the lowest two transform from the Neumann case into their Dirichlet counterparts, and the subsequent growth of the de Gennes distance to the large positive values forces them to convert again into the Neumann states located, however, two subbands below the corresponding levels at Λ=−∞. The two lowest at Λ=−∞ thresholds come closer to each other and tend to the negative large values as the extrapolation length approaches zero from the left. From Eq. (21a) it can be

shown that the energy of the higher split-off level which was positive at $\Lambda=-\infty$ crosses zero at the following relation between Λ_{in} and Λ_{out}

$$\frac{\Lambda_{in}}{\rho_0}+\frac{\Lambda_{out}}{\rho_0+1}+\ln\left(1+\frac{1}{\rho_0}\right)=0. \tag{22}$$

As in the previous cases, Eq. (22) at $\rho_0\to\infty$ turns into its straight counterpart, Eq. (12). For the symmetric case, $\Lambda_{in}=\Lambda_{out}=\Lambda$, it simplifies to

$$\Lambda|_{E_{TH}=0}=-\frac{\rho_0(\rho_0+1)}{2\rho_0+1}\ln\left(1+\frac{1}{\rho_0}\right) \tag{23}$$

what in the case of Fig. 3 is equal to $\Lambda=-0.2198$.

Radial functions of the several low-lying states are plotted in the right inset. It is seen that, contrary to the Cartesian geometry when both negative levels are equally shared by the two film boundaries, the lowest level is mainly localized near the outer surface while its higher-lying split-off counterpart occupies the area near the inner interface. This difference can be easily explained: for the straight film the upward motion does not have any preferences compared to the downward one (and vice versa) while in the curved channel the motion in the direction of increasing radius is not equivalent to its opposite counterpart. Semiclassically, this difference is due to the centrifugal forces acting in the bend [83] and being absent in the straight arms. Thus, a bend perturbation of the straight film allows one to spatially separate the split-off surface states induced by the negative Robin parameter. This also explains the smaller degree of degeneracy of the negative-energy levels at the same Λ.

Similar to the straight wire, positive-energy thresholds are located in the bulk. Function of the nth state has $(n-1)$ nodes; however, its symmetry or antisymmetry with respect to the middle of the bend is lost what again is explained by the curvature-induced centrifugal forces.

For comparison, we also plot in the left inset of Fig. 3 the corresponding $E_{TH}-\Lambda$ dependence for the zero-radius bend when Eqs. (18), (20), and (21) transform into Eqs. (24)–(26), respectively,

$$R_{\nu_n}(\rho)=Q_nJ_{\nu_n}(\pi\sqrt{E}\rho),\quad E>0, \tag{24a}$$

$$R_{\nu_n}(\rho)=Q_nI_{\nu_n}(\pi\sqrt{|E|}\rho),\quad E<0, \tag{24b}$$

$$\pi\sqrt{E}J'_{\nu_n}(\pi\sqrt{E})+\frac{1}{\Lambda_{out}}J_{\nu_n}(\pi\sqrt{E})=0,\quad E>0, \tag{25a}$$

$$\pi\sqrt{|E|}I'_{\nu_n}(\pi\sqrt{|E|})+\frac{1}{\Lambda_{out}}I_{\nu_n}(\pi\sqrt{|E|})=0,\quad E<0, \tag{25b}$$

$$-\pi\sqrt{E_{TH}}J_1(\pi\sqrt{E_{TH}})+\frac{1}{\Lambda_{out}}J_0(\pi\sqrt{E_{TH}})=0,\quad E_{TH}>0, \tag{26a}$$

$$\pi\sqrt{|E_{TH}|}I_1(\pi\sqrt{|E_{TH}|})+\frac{1}{\Lambda_{out}}I_0(\pi\sqrt{|E_{TH}|})=0,\quad E_{TH}<0. \tag{26b}$$

In this case, only one—outer—surface exists. Accordingly, one can expect that only one split-off level will emerge as the extrapolation length tends to zero from the left. This is exactly what is seen in the plot. In turn, the higher-lying thresholds gradually change their $(n-1)$th Neumann behavior via the $(n-2)$th Dirichlet threshold at $\Lambda=0$ into the $(n-2)$th Neumann state as the extrapolation length runs along the increasing Λ axis. Change by *one* subband is, once again, explained by only *one* confining surface. As it straightforwardly follows from Eq. (24b) and the properties [79] of the modified Bessel function $I_\nu(\rho)$, the corresponding function of the negative-energy level is localized near the circumference of the bend what authorizes to call it a surface state [18,24]. For the straight geometry it is impossible to confine the particle by one surface only; however, the external magnetic field parallel to the single plate overcomes this difficulty. On the numerical note, we note that for all extrapolation lengths the fundamental propagation threshold for the straight channel always possesses a larger—either negative or positive, depending on the sign of Λ—energy E_{TH} compared to its bend counterpart with this difference increasing for the decreasing radius ρ_0 what means, according to the GL theory, higher critical temperature T for the curved wire and either sign of Λ. This is consistent with previous theoretical findings [13,14]. In turn, for the higher-lying thresholds and the negative Λ the situation is reversed while for the positive extrapolation lengths the situation is even more intricate when the larger slope of the straight-arm thresholds allows them to cross the curved section subband boundaries at the radius-dependent Robin parameters and at large positive Λ to lie below them with the difference increasing for the smaller ρ_0.

In a standard manner, one can define scattering **S** and reflection **R** matrices of the structure which link, respectively, the amplitudes of the transmitted or reflected waves in each subband with those of the incident flux,

$$\mathbf{C}=\mathbf{SA}, \tag{27a}$$

$$\mathbf{B}=\mathbf{RA}, \tag{27b}$$

where the amplitudes A_n, B_n, and C_n from Eqs. (6) and (7) form infinite column vectors **A**, **B**, and **C**, respectively. For the ferromagnetic arrangement, scattering matrix **S** defines the conductance G of the strip [84],

$$G(E)=\sum_{nn'}\frac{k_n}{k_{n'}}|S_{nn'}|^2, \tag{28}$$

where the sum runs over all open channels. The same formula can be used for calculating the power transmission ratio of the metallic waveguide with ferrite inside. Also, $|S_{11}|^2$ defines a transmission through the bend in the fundamental propagating mode of the superconducting film. The relation between scattering and reflection matrices reads,

$$\sum_{nn'} \frac{k_n}{k_{n'}}(|S_{nn'}|^2 + |R_{nn'}|^2) = N_o, \tag{29}$$

with N_o being a number of open channels. To find the coefficients $S_{nn'}$ and $R_{nn'}$, one needs to match solutions in different regions. This is done with the help of the following relations [59]:

$$(x=0,y) \Leftrightarrow (\rho_0 + y, \varphi = 0), \tag{30a}$$

$$(x_1=0,y_1) \Leftrightarrow (\rho_0 + y_1, \varphi = \varphi_0), \tag{30b}$$

$$\left.\frac{\partial}{\partial x}\right|_{x=0} \Leftrightarrow \left.\frac{1}{\rho_0 + y}\frac{\partial}{\partial \varphi}\right|_{\varphi=0}, \tag{30c}$$

$$\left.\frac{\partial}{\partial x_1}\right|_{x_1=0} \Leftrightarrow \left.\frac{1}{\rho_0 + y_1}\frac{\partial}{\partial \varphi}\right|_{\varphi=\varphi_0}, \tag{30d}$$

linking coordinate systems (x,y), (ρ,φ), and (x_1,y_1). After matching, one arrives at the following system:

$$\sum_{n=1}^{\infty} (A_n + B_n)\chi_n(y) = \sum_{n=1}^{\infty} (D_n + F_n)R_{\nu_n}(\rho_0 + y), \tag{31a}$$

$$\sum_{n=1}^{\infty} k_n(A_n - B_n)\chi_n(y) = \frac{1}{\rho_0 + y}\sum_{n=1}^{\infty} \nu_n(D_n - F_n)R_{\nu_n}(\rho_0 + y), \tag{31b}$$

$$\sum_{n=1}^{\infty} C_n\chi_n(y_1) = \sum_{n=1}^{\infty} (D_n e^{i\nu_n\varphi_0} + F_n e^{-i\nu_n\varphi_0})R_{\nu_n}(\rho_0 + y_1), \tag{31c}$$

$$\sum_{n=1}^{\infty} k_n C_n\chi_n(y_1) = \frac{1}{\rho_0 + y_1}\sum_{n=1}^{\infty} \nu_n(D_n e^{i\nu_n\varphi_0} - F_n e^{-i\nu_n\varphi_0}) \times R_{\nu_n}(\rho_0 + y_1). \tag{31d}$$

System of Eqs. (31) allows one to express the coefficients C_n and B_n through A_n, what, according to Eqs. (27), means a calculation of the scattering and reflection matrices. They will include integrals

$$\int_0^1 \chi_n(y)R_{\nu_{n'}}(\rho_0 + y)dy, \tag{32a}$$

$$\int_0^1 \chi_n(y)R_{\nu_{n'}}(\rho_0 + y)dy/(\rho_0 + y). \tag{32b}$$

In known to us literature [79,85–87] there are no analytical expressions for such integrals; accordingly, we performed their direct numerical quadrature. We note here in passing that even though integral from Eq. (19) has its analytical expression [79,85,86], we nevertheless also calculated it numerically since its analytical expression includes Bessel function derivative with respect to its index what is not the best way to realize computationally.

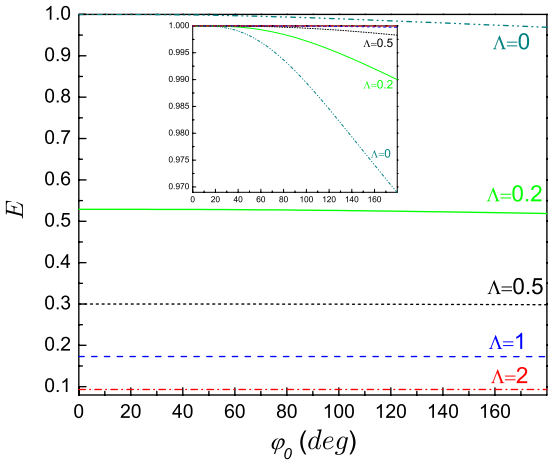

FIG. 4. (Color online) Bound-state energies E as a function of the bend angle φ_0 for $\rho_0=0.1$ and several positive extrapolation lengths Λ, where the solid line is for $\Lambda=0.2$, the dotted line is for $\Lambda=0.5$, the dashed line is for $\Lambda=1$, and the dash-dotted line is for $\Lambda=2$. For comparison, the case of pure Dirichlet condition, $\Lambda=0$, is also shown (dash-dot-dotted line). The inset shows the same states offset, for clarity, to match the energies at $\varphi_0=0$ and $\Lambda=0$. Note different energy scales in the main figure and the inset.

When one is looking for the bound-state energies lying below the fundamental propagation threshold of the straight arm, it is necessary to put all coefficients A_n in Eq. (6) equal to zero which naturally means that there are no any incoming modes. Then, as a result of matching, one gets the infinite linear algebraic system. Requirement of vanishing of its determinant defines energies of the bound levels. An infinite set of eigenvectors corresponding to the eigenenergies defines coefficients B_n, D_n, F_n, and C_n what allows to fully construct bound-state wave function.

III. RESULTS AND DISCUSSION

Here we present results of the theory developed in the previous section with their detailed analysis. We start from the description of the bound states. Figure 4 shows bound-state energies E as a function of the bend angle φ_0 for $\rho_0=0.1$ and several non-negative extrapolation lengths. As our analysis shows, for the symmetric case of the equal Robin parameters on both confining surfaces, the split-off level below the first transversal mode exists for all bend parameters; in particular, arbitrary small angles φ_0 are able to support it. Since, as it follows from Fig. 2, the fundamental thresholds decrease with increasing Λ, the curves for the larger Λ are located below those with the smaller length

$$E(\varphi_0,\Lambda_1) \geq E(\varphi_0,\Lambda_2), \quad \Lambda_1 \leq \Lambda_2. \tag{33}$$

From the fundamental propagation threshold at $\varphi_0=0$, the energies for all lengths monotonically decrease with increasing the bend angle. In Fig. 4, we confined our consideration to the physically relevant situation of $0° \leq \varphi_0 \leq 180°$; however, for the arbitrary unrealistically large angle $\varphi_0 \geq \pi$ they tend to zero as $\varphi_0 \to \infty$. To elucidate the φ_0-dependence in more detail, we depict in the inset of Fig. 4 the same energies

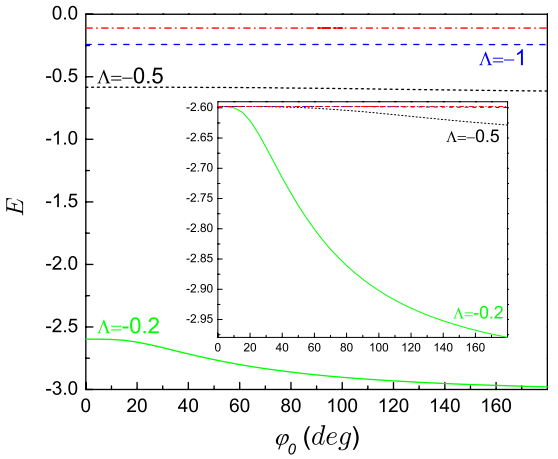

FIG. 5. (Color online) Same as in Fig. 4 but for the negative extrapolation lengths: the solid line is for $\Lambda=-0.2$, the dotted line is for $\Lambda=-0.5$, the dashed line is for $\Lambda=-1$, and the dash-dotted line is for $\Lambda=-2$. The inset shows the same levels offset, for clarity, to match the energies at $\varphi_0=0$ and $\Lambda=-0.2$.

offset to match that of the Dirichlet case at zero bend angle. It clearly shows that the ground-state-energy slope, $\partial E/\partial\varphi_0$, is stronger for the more Dirichlet-like situation,

$$\left.\frac{\partial E}{\partial \varphi_0}\right|_{\Lambda_1} \leq \left.\frac{\partial E}{\partial \varphi_0}\right|_{\Lambda_2}, \quad \Lambda_1 \geq \Lambda_2. \tag{34}$$

With the growing extrapolation length, the bound-state energy E is less and less φ_0-dependent until at $\Lambda=+\infty$ this split-off level merges with the zero energy fundamental propagation threshold and in this way ceases to exist.

As Fig. 5 shows, basically the same features are observed for the negative Robin parameters; in particular, inequalities (33) and (34) also hold.

Figure 6 shows bound-state energies as a function of the bend angle for $\Lambda=0.3$ and several bend radii. It is seen that the energies for the smaller ρ_0 deviate downward stronger

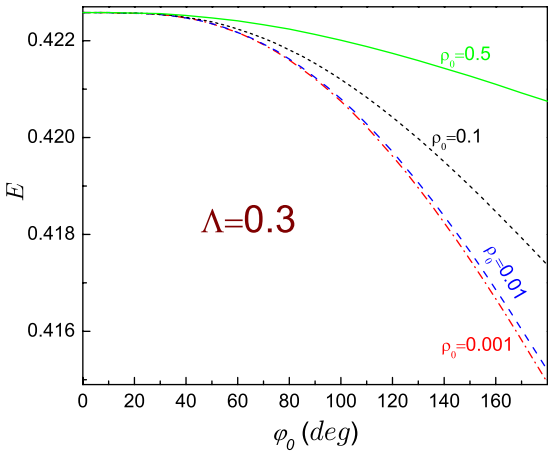

FIG. 6. (Color online) Bound-state energies E as a function of the bend angle φ_0 for $\Lambda=0.3$ and several bend radii ρ_0, where the solid line is for $\rho_0=0.5$, the dotted line is for $\rho_0=0.1$, the dashed line is for $\rho_0=0.01$, and the dash-dotted line is for $\rho_0=0.001$.

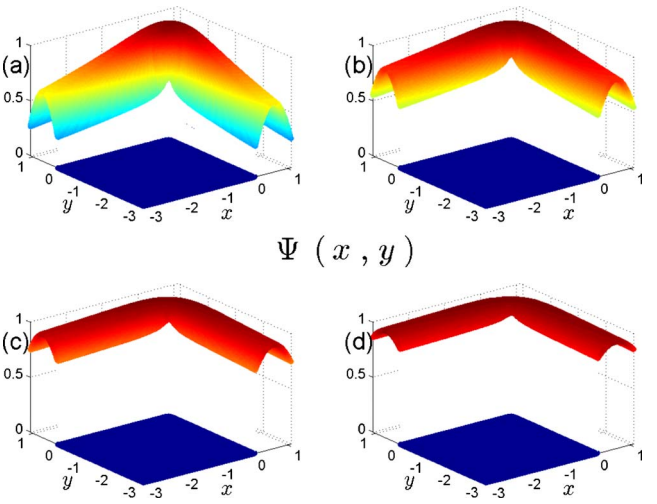

FIG. 7. (Color online) Order parameter $|\Psi(x,y)|$ (normalized to its maximum) of the bound state for $\rho_0=0.1$, the right angle and several positive extrapolation lengths: (a) $\Lambda=0.2$, (b) $\Lambda=0.5$, (c) $\Lambda=1$, and (d) $\Lambda=2$. Here, the origin of the Cartesian system (x,y) coincides with the center of the bend.

compared to the bend with larger radius. Explanation of this is the same as for the pure Dirichlet [57] or Dirichlet-Neumann [64] case; namely, a smaller radius presents a stronger perturbation to the particle in the straight part, and so, its energy is more affected and moves more downward from the threshold of the straight arm. For the very small radii a further decrease in ρ_0 does not bring much difference; so, the curves for $\rho_0=0.01$ and $\rho_0=0.001$ are very close to each other.

Figures 7 and 8 show bound-state order parameter $\Psi(x,y)$ for several positive and negative extrapolation lengths, respectively, with $\rho_0=0.1$ and the right angle. For small $|\Lambda|$ the function is mainly localized in the bend quickly decaying in the straight arms. As the waveguide becomes more Neumannian, the order parameter decreases its longitudinal as well as

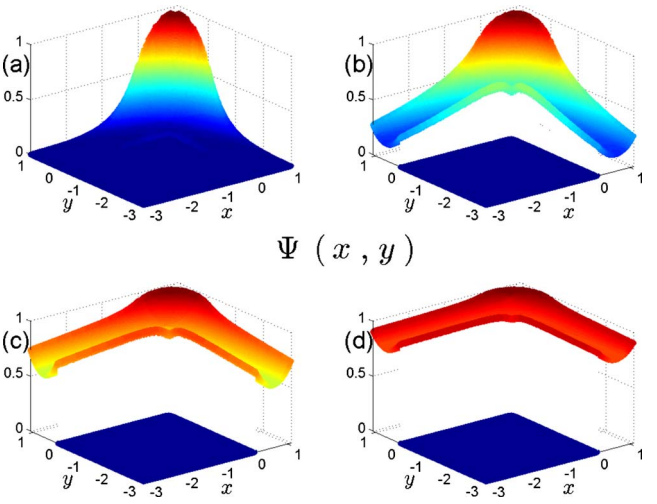

FIG. 8. (Color online) Same as in Fig. 7 but for the negative extrapolation lengths: (a) $\Lambda=-0.2$, (b) $\Lambda=-0.5$, (c) $\Lambda=-1$, (d) $\Lambda=-2$.

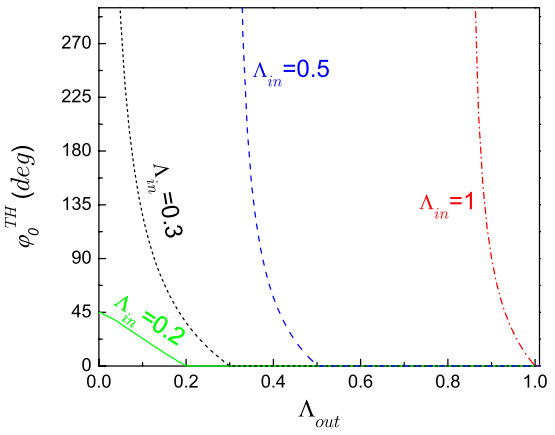

FIG. 9. (Color online) Threshold angle φ_0^{TH} at which the bound state emerges from the continuum as a function of Λ_{out} and several Λ_{in} where the solid curve is for $\Lambda_{in}=0.2$, the dotted line is for $\Lambda_{in}=0.3$, the dashed curve is for $\Lambda_{in}=0.5$, and the dash-dotted line is for $\Lambda_{in}=1$. Bend radius is $\rho_0=0.1$.

transverse slopes, and at $|\Lambda|\to\infty$ it becomes completely flat since its energy coincides with the fundamental propagation threshold of the Neumann waveguide, i.e., it becomes zero. For all bend angles and extrapolation lengths, the order parameter is symmetric with respect to the plane $\varphi=\varphi_0/2$. Note different slopes of the function for the opposite signs of the extrapolation length: if, for the positive Robin parameter, the transverse profile has its maximum in the middle of the duct both in the bend as well as in the straight part, the situation is different for the negative length where maxima are achieved at the waveguide walls. The easiest way to explain this is again the reference to the superconductor language; namely, a positive Λ means a suppression of the superconductivity in the duct by the external environment; accordingly, nucleation of the waveguide superconductivity takes place in its middle part. In turn, the negative Robin lengths mean that the channel superconductivity is enhanced by its surroundings and so, the order parameter is attracted to the duct walls, as Fig. 8 exemplifies.

So far, we have considered the same Robin parameters on both walls. It is interesting to investigate the case of different Λ and their influence on the bound states. Figure 9 shows the threshold angle φ_0^{TH} at which the localized level emerges from the continuum. Our results manifest that the bound state exists at any infinitely small angle if $\Lambda_{out}\geq\Lambda_{in}$. However, as long as the outer extrapolation length gets smaller than the inner one, a threshold angle at which the bound levels appears, takes nonzero value. The angle increases with the difference between Λ_{in} and Λ_{out} while the slope of the curve gets steeper with Λ_{in} increasing. In other words, the waveguide bend with different parameters can bind the wave inside only if the outer length is not smaller than the inner one. In the opposite case the bend in some length-dependent angle range is not "strong" enough and cannot trap the particle until the angle passes some critical threshold, and with this help the bound state can be created. In terms of the straightening transformation [56] it means that for the inner extrapolation length being less than the outer one the bend creates a symmetric effective attractive potential in the

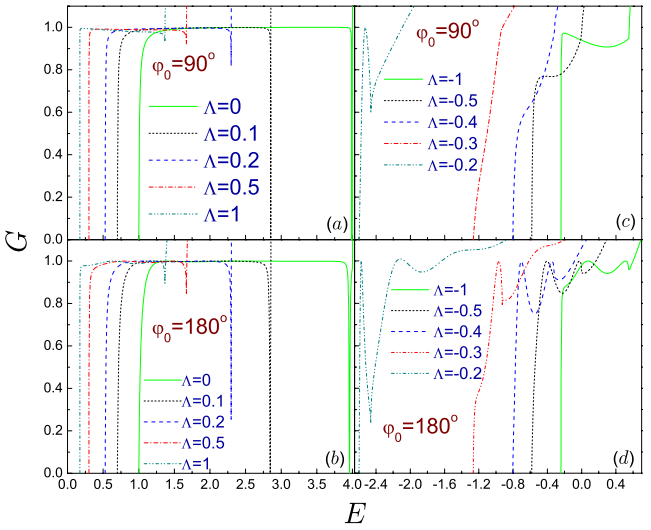

FIG. 10. (Color online) Conductance G as a function of energy E for the film with radius $\rho_0=0.1$ and bend angles (a), (c) $\varphi_0=90°$ and (b), (d) $\varphi_0=180°$. Panels (a) and (b) show transmissions for the positive extrapolation lengths where the dotted lines are for $\Lambda=0.1$, the dashed lines are for $\Lambda=0.2$, the dash-dotted lines are for $\Lambda=0.5$, and the dash-dot-dotted lines are for $\Lambda=1$. For comparison, the cases of a pure Dirichlet ($\Lambda=0$) waveguide are also shown (solid lines). Panels (c) and (d) exhibit transmissions for the negative extrapolation lengths with solid lines depicting the case of $\Lambda=-1$, dotted lines—$\Lambda=-0.5$, dashed lines—$\Lambda=-0.4$, dash-dotted lines—$\Lambda=-0.3$, and dash-dot-dotted lines—$\Lambda=-0.2$. Note different energy ranges for the left and right panels.

straight waveguide when the bound state always exists [6] while in the opposite case the effective negative bend-induced potential well is an asymmetric one and for the small angles φ_0 its width proportional to ρ_0 and φ_0 does not allow to bind a particle [6]. The conclusion that the bound state exists for any angle if the outer surface is more Neumannian than the inner one, is consistent with the previous studies [63–65] which showed, as we already mentioned, that the localized level exists for the inner Dirichlet and outer Neumann boundaries. Here we generalized this statement to the arbitrary Robin lengths.

Next, we turn to the scattering case. In Fig. 10 we plot conductances G for $\rho_0=0.1$, two angles $\varphi_0=90°$ and $\varphi_0=180°$ and several positive and negative lengths. We mainly confined our consideration to the fundamental propagating subband in order not to obscure the picture by the interference effects between different modes. For positive Robin parameter the increasing Λ shifts the conductance curve to the smaller energies simultaneously gradually eliminating antiresonance which, in the Dirichlet case, was caused by the interaction of the split-off level of the higher subband with the continuum states of the fundamental propagating mode. It is seen that the dip at $\Lambda=0.1$ persists to retain its zero minimum what can be attributed to the fact that the first excited propagation threshold for the bend is still smaller than its value in the straight arm; however, for the larger extrapolation lengths when the thresholds exchange their mutual locations, its minimum G_{min} surrenders to the increasing influence of the growing length and acquires non-

zero value which increases with Λ. At the large lengths this antiresonance is completely dissolved transforming propagation curve into the pure Neumann case. As panels (a) and (b) show, this elimination has different speeds for the different bend angles. One can draw parallels here to the uniform magnetic field influence on the transmission of the Dirichlet curved waveguide [62]. In both cases an increasing parameter—either the extrapolation length or magnetic field—leads to the ultimate dissolution of the antiresonance; however, the details of such disappearance essentially differ: in the latter case the conductance in the minimum is an oscillating several times function of the field and reaches zero again a finite bend-dependent number of times while the increase in the extrapolation length causes a smooth washing out of the dip. Energy directions in which the modified antiresonance moves are also different: smaller one for the length and larger for the field. The same statement applies also to the widths of the final subbands. Such differences present a foundation for the investigation of the simultaneous influence of both these forces on the properties of the bent waveguide.

For the small negative lengths, as we already mentioned before, the fundamental propagating mode lies in the negative-energy range with its width decreasing when Λ approaches zero. Even though the energy is negative, the transport here can be considered as a tunneling current [13,14]. There is no any antiresonances characteristic for the positive Robin coefficient. One sees some Breit-Wigner-like resonances with their number increasing for the larger angle. It can be attributed to the larger resonator length formed by the junctions of the bent section with the straight arms. In the Λ range shown in the figure, this number also increases with the growing absolute value of the extrapolation length. However, for the larger length magnitude when $\Lambda \to -\infty$ these resonances disappear transforming into the straight subband boundaries of the Neumann case.

IV. CONCLUDING REMARKS

A theoretical analysis of the curved planar waveguide subjected to the Robin interface requirements, Eq. (2), is a generalization of the previous studies with either pure Dirichlet, or Neumann, or Dirichlet-Neumann distribution of the boundary conditions. It was revealed that the bound state below the fundamental transverse mode always exists if the external extrapolation length is not smaller than the inner one. In the opposite case there is a range of the bend parameters where the curved section is too "weak" to bind the wave inside it. This generalized condition of the bound-state existence is in agreement with the previous conclusion of the particular case of the opposite surfaces with the different—either Dirichlet or Neumann—surface requirements.

In our present treatment we mainly confined the bend angle φ_0 to the physically relevant situation of $0° \le \varphi_0 \le 180°$. It is known that for the pure Dirichlet [88] or Dirichlet-Neumann [64] waveguides multiple bound states emerge at the larger angles with alternating symmetric/antisymmetric properties. Since the same behavior for the Robin waveguide is very similar to these cases described before [64,88], we omitted their discussion in the present consideration.

As we stated in the Introduction, developed here formalism of the linear Helmholtz equation is straightforwardly applicable to the analysis of the magnetic multilayers and ferrite-filled metallic waveguides. A treatment of the bound states aiming at the finding the critical temperature of the curved superconducting film is also governed by the linearized GL equation with the theoretical predictions being in a very good agreement with the experiment (for review, see Ref. [89]). However, for the correct description of the scattering case in the superconducting films one needs to add the term $\beta|\Psi|^2\Psi$ to the left-hand side of Eq. (3). Here, the second GL parameter β for the "pure" superconductors in the dimensional units is written as [4,8]

$$\beta \simeq \frac{1}{N(0)}\left[\frac{\hbar^2}{2m\xi^2(0)}\right]^2 \frac{1}{(k_B T_c)^2} \tag{35}$$

with $N(0)$ being the density of states at the Fermi energy and k_B being the Planck constant. For the "dirty" superconductors (alloys), $\xi^2(0)$ in the GL parameters α and β should be substituted by $\xi(0)l$, with l being the mean free path of the material. Introduction of the cubic term drastically complicates theoretical treatment; for example, in the straight arm a solution Ψ is expressed via the elliptic sine $\mathrm{sn}(u|m)$ [79] with nontrivial arguments [7,10]. To justify at least qualitative survival of the results of the linearized theory developed above, we repeat the arguments already put forward for the Dirichlet-Neumann case [67]. First, a manipulation of the parameters $N(0)$, $\xi(0)$, and T_c in Eq. (35) by the appropriate choice of the material can significantly reduce the GL term β. Also, it was shown by the numerical calculation [90] that the linearized GL equation correctly captures features of the aluminum disks of the different radii, especially for the small ρ_0 when the predictions of the full GL theory are in a worse agreement with the experiment [91] than the results produced by the solution of Eq. (3). Both the experiment [91] and its theoretical explanation [90] are carried out to the temperatures of $T=0.4$ K lying well below corresponding $T_c=1.19$ K for aluminum (cf. Ref. [4]). In our scattering configuration such a ratio for $\xi(0)=120$ nm [92] and $d=1$ μm corresponds to the dimensionless energy $E \sim 5$ what for $\Lambda \sim 0.3-0.5d$ is in the neighborhood of the upper threshold of the first excited propagating mode. All this leads us to believe that the results of the present research of the scattering configuration will survive—at least, qualitatively,—in more elaborated calculations and in the experiment.

Let us make more numerical estimates. For the straight film of the thickness $d=1$ μm with the typical aluminum coherence length $\xi(0)=120$ nm [92] the negative dimensionless extrapolation length $\Lambda=-0.2$ leads to the lowest propagation threshold $E_{TH}=-2.5979$, what, in turn, according to Eq. (5), turns the ratio T/Tc equal to 1.369. Bending of the film by the right angle and bend radius $\rho_0=d/10$ decreases bound-state dimensionless energy to $E=-2.8932$ what increases the actual critical temperature to the ratio $T/Tc=1.411$. This means an increase of 3% compared to the straight film. Further bending by the angle $\varphi_0=180°$ decreases the dimensionless energy to $E=-2.9795$ what leads

to the ratio $T/Tc=1.423$ and stands for 4% increase as for the straight channel. Even more gain can be achieved for the smaller bend radii, as Fig. 6 demonstrates. It was argued [15] that the negative extrapolation length can be controlled by changing the abrasive sample grain size and the annealing time and temperature. It can also be manipulated by the electric field [17]. It opens up possibilities of a quite wide variation of the critical temperature by either the preparation processes or/and external factors.

Finally, we point out again that discussed in the present research *real* Robin parameter is a particular case of the more general situation of the *complex* Λ. As it was stated in the Introduction, the latter case describes lined acoustical channels [73–77] where the extrapolation length is expressed via the *complex* acoustical impedance which means the reacting absorbing waveguide interfaces. It is known that in the electromagnetic waveguides without parameter dependence on the in-plane tangential direction the very similar boundary conditions occur too [93]; however, a situation is even more intricate here since the parameter Λ in this case depends not only on the *complex* electromagnetic surface impedance but also on the eigenvalue ε from Eq. (1) which enters the extrapolation length via the product (or division) with the impedance [93]. It was shown that the introduction of the nonzero imaginary part into the Robin parameter is equivalent to the sound attenuation during its propagation down the channel [74–76], and the magnitude of the attenuation was discussed for the different bend parameters and frequencies. While the transport properties of the complex-Λ curved structures were analyzed, an open question still remains a problem of the bound-state existence under the same boundary requirements. It is of interest to find out the conditions for the localized-mode existence in this case and its dependence on the correlation between the real and imaginary parts of the complex Robin parameter Λ. Such calculations are now in progress and will be reported elsewhere.

ACKNOWLEDGMENTS

O.O. acknowledges hospitality of the Department of Physics, Jackson State University, Jackson, MS, USA where a portion of this project was done with the partial financial support from NSF under Grant No. DMR-0606509 and from DoD under Contract No. W912HZ-06-C-0057.

[1] K. Gustafson and T. Abe, Math. Intell. **20**, 63 (1998).
[2] P. M. Morse and H. Feshbach, *Methods of Theoretical Physics* (McGraw-Hill, New York, 1953), Part II, Chap. 9.2.
[3] V. L. Ginsburg and L. D. Landau, Zh. Eksp. Teor. Fiz. **20**, 1064 (1950).
[4] P. G. de Gennes, *Superconductivity of Metals and Alloys* (Benjamin, New York, 1966).
[5] L. D. Landau and E. M. Lifshitz, *Statistical Physics* (Pergamon, New York, 1980), Part 2.
[6] L. D. Landau and E. M. Lifshitz, *Quantum Mechanics (Non-relativistic Theory)* (Pergamon, New York, 1977).
[7] E. A. Andryushin, V. L. Ginzburg, and A. P. Silin, Usp. Fiz. Nauk **163** (9), 105 (1993) [Phys. Usp. **36**, 854 (1993)]; Usp. Fiz. Nauk **163** (11), 102 (1993) [Phys. Usp. **36**, 1086 (1993)].
[8] L. P. Gor'kov, Zh. Eksp. Teor. Fiz. **36**, 1918 (1959) [Sov. Phys. JETP **9**, 1364 (1959)].
[9] R. O. Zaĭtsev, Zh. Eksp. Teor. Fiz. **48**, 644 (1965) [Sov. Phys. JETP **21**, 426 (1965)]; Zh. Eksp. Teor. Fiz. **50**, 1055 (1966) [Sov. Phys. JETP **23**, 702 (1966)].
[10] R. O. Zaĭtsev, Zh. Eksp. Teor. Fiz. **48**, 1759 (1965) [Sov. Phys. JETP **21**, 1178 (1965)].
[11] A. A. Abrikosov, Zh. Eksp. Teor. Fiz. **47**, 720 (1964) [Sov. Phys. JETP **20**, 480 (1965)].
[12] H. J. Fink and W. C. H. Joiner, Phys. Rev. Lett. **23**, 120 (1969).
[13] E. Montevecchi and J. O. Indekeu, Europhys. Lett. **51**, 661 (2000).
[14] E. Montevecchi and J. O. Indekeu, Phys. Rev. B **62**, 14359 (2000).
[15] V. F. Kozhevnikov, M. J. Van Bael, W. Vinckx, K. Temst, C. Van Haesendonck, and J. O. Indekeu, Phys. Rev. B **72**, 174510 (2005).
[16] I. N. Khlyustikov and A. I. Buzdin, Adv. Phys. **36**, 271 (1987).
[17] P. Lipavský, K. Morawetz, J. Koláček, and T. J. Yang, Phys. Rev. B **73**, 052505 (2006); J. Koláček, P. Lipavský, K. Morawetz, and E. H. Brandt, *ibid.* **79**, 174510 (2009).
[18] R. Balian and C. Bloch, Ann. Phys. **60**, 401 (1970).
[19] B. D. Sleeman and E. M. E. Zayed, J. Math. Anal. Appl. **94**, 78 (1983); E. M. E. Zayed, *ibid.* **112**, 455 (1985); Houst. J. Math **24**, 377 (1998); Acta Math. Sin. English Ser. **16**, 627 (2000); IMA J. Appl. Math. **64**, 95 (2000); Appl. Math. Comput. **132**, 515 (2002).
[20] M. Sieber, H. Primack, U. Smilansky, I. Ussishkin, and H. Schanz, J. Phys. A **28**, 5041 (1995); K. Hornberger and U. Smilansky, *ibid.* **33**, 2829 (2000); Phys. Rep. **367**, 249 (2002).
[21] E. N. Dancer and D. Daners, J. Differ. Equ. **138**, 86 (1997); D. Daners, Trans. Am. Math. Soc. **352**, 4207 (2000); D. Daners and J. Kennedy, SIAM J. Math. Anal. **39**, 1191 (2007).
[22] D. I. Borisov and R. R. Gadyl'shin, Teor. Mat. Fiz. **118**, 347 (1999) [Theor. Math. Phys. **118**, 272 (1999)]; C. R. Acad. Sci. Paris Ser. IIB Mechanics **329**, 717 (2001); Mat. Sb. **193** (7), 37 (2002) [Sb. Math. **193**, 977 (2002)]; Asymptotic Anal. **35**, 1 (2003); Izv. RAN Ser. Mat. **67** (6), 23 (2003) [Izv. Math. **67**, 1101 (2003)]; Sib. Mat. Zh. **45**, 272 (2004) [Sib. Math. J. **45**, 222 (2004)]; Zh. Vych. Mat. Mat. Fiz. **46**, 284 (2006) [Comput. Math. Math. Phys. **46**, 271 (2006)].
[23] W. Arendt and M. Warma, J. Evol. Equ. **3**, 119 (2003); Potential Anal. **19**, 341 (2003).
[24] M. V. Berry and M. R. Dennis, J. Phys. A **41**, 135203 (2008).
[25] M. Marlettta and G. Rozenblum, J. Phys. A **42**, 125204 (2009).
[26] M. V. Berry, J. Phys. A **42**, 165208 (2009).
[27] P. Exner and S. A. Vugalter, Ann. Inst. Henri Poincare, Sect. A **65**, 109 (1996).
[28] W. Bulla, F. Gesztezy, W. Renger, and B. Simon, Proc. Am. Math. Soc. **125**, 1487 (1997).

[29] E. B. Davies and L. Parnovski, Q. J. Mech. Appl. Math. **51**, 477 (1998).
[30] D. Borisov, P. Exner, and R. Gadyl'shin, J. Math. Phys. **43**, 6265 (2002).
[31] J. Dittrich and J. Kříž, J. Math. Phys. **43**, 3892 (2002); H. Kovařík and D. Krejčiřík, Math. Nachr. **281**, 1159 (2008).
[32] D. Borisov and P. Exner, J. Phys. A **37**, 3411 (2004).
[33] O. Olendski and L. Mikhailovska, J. Phys. A **40**, 4609 (2007).
[34] H. Najar, S. Ben Hariz, and M. Ben Salah, Math. Phys. Anal. Geom. **13**, 19 (2010).
[35] B. J. Baelus, B. Partoens, and F. M. Peeters, Phys. Rev. B **73**, 212503 (2006).
[36] M. Jílek, Symmetry, Integr. Geom.: Methods Appl. **3**, 108 (2007).
[37] G. Richardson and J. Rubinstein, Appl. Math. Lett. **13** (3), 97 (2000).
[38] X.-B. Pan, SIAM J. Math. Anal. **34**, 957 (2003).
[39] I. Y. Popov and E. S. Tesovskaya, Teor. Mat. Fiz. **146**, 429 (2006) [Theor. Math. Phys. **146**, 361 (2006)]; L. V. Gortinskaya, I. Y. Popov, E. S. Tesovskaya, and V. M. Uzdin, Physica E (Amsterdam) **36**, 12 (2007).
[40] W. Rostafinski, *Monograph on Propagation of Sound Waves in Curved Ducts* (NASA Scientific and Technical Information Division, Washington, D.C., 1991).
[41] S. Félix and V. Pagneux, J. Acoust. Soc. Am. **110**, 1329 (2001).
[42] J. A. Cochran and R. G. Pecina, Radio Sci. **1**, 679 (1966).
[43] L. Lewin, D. C. Chang, and E. F. Kuester, *Electromagnetic Waves and Curved Structures* (Peter Peregrinus, Stevenage, UK, 1977).
[44] B. Z. Katsenelenbaum, L. Mercader del Río, M. Pereyaslavets, M. Sorolla Ayza, and M. Thumm, *Theory of Nonuniform Waveguides* (IEE, London, UK, 1998).
[45] P. Duclos and P. Exner, Rev. Math. Phys. **7**, 73 (1995).
[46] J. T. Londergan, J. P. Carini, and D. P. Murdock, *Binding and Scattering in Two-Dimensional Systems: Applications to Quantum Wires, Waveguides, and Photonic Crystals* (Springer-Verlag, Berlin, 1999).
[47] F. Lenz, J. T. Londergan, E. J. Moniz, R. Rosenfelder, M. Stingl, and K. Yazaki, Ann. Phys. (N.Y.) **170**, 65 (1986).
[48] H. M. Hulburt and J. O. Hirschfelder, J. Chem. Phys. **11**, 276 (1943); K. T. Tang, B. Kleinman, and M. Karplus, *ibid.* **50**, 1119 (1969); P. D. Robinson, *ibid.* **52**, 3175 (1970); D. R. Dion, M. B. Milleur, and J. O. Hirschfelder, *ibid.* **52**, 3179 (1970); J. O. Hirschfelder and K. T. Tang, *ibid.* **64**, 760 (1976).
[49] H. Eyring, J. E. Walter, and G. E. Kimball, *Quantum Chemistry* (Wiley, New York, 1944), Chap. 16.
[50] M. Jouguet, Ann. Telecommun. **2**, 78 (1947); Cables Transm. **1**, 39 (1947).
[51] V. P. Maslov, Dokl. Akad. Nauk SSSR **123**, 631 (1958) [Sov. Phys. Dokl. **3**, 1132 (1959)]; V. P. Maslov and E. M. Vorob'ev, Dokl. Akad. Nauk SSSR **179**, 558 (1968) [Sov. Phys. Dokl. **13**, 223 (1968)].
[52] C. P. Bates, Bell Syst. Tech. J. **49**, 2259 (1969).
[53] P. Exner and P. Šeba, J. Math. Phys. **30**, 2574 (1989).
[54] R. L. Schult, D. G. Ravenhall, and H. W. Wyld, Phys. Rev. B **39**, 5476 (1989).
[55] J. Goldstone and R. L. Jaffe, Phys. Rev. B **45**, 14100 (1992).
[56] D. W. L. Sprung, H. Wu, and J. Martorell, J. Appl. Phys. **71**, 515 (1992).
[57] F. Sols and M. Macucci, Phys. Rev. B **41**, 11887 (1990).
[58] P. Duclos, P. Exner, and P. Šťovíček, Ann. Inst. Henri Poincare, Sect. A **62**, 81 (1995).
[59] O. Olendski and L. Mikhailovska, Phys. Rev. B **66**, 035331 (2002).
[60] J. P. Carini, J. T. Londergan, K. Mullen, and D. P. Murdock, Phys. Rev. B **46**, 15538 (1992); **48**, 4503 (1993); J. P. Carini, J. T. Londergan, D. P. Murdock, D. Trinkle, and C. S. Yung, *ibid.* **55**, 9842 (1997).
[61] J. von Neumann and E. Wigner, Phys. Z. **30**, 465 (1929); S. Albeverio, Ann. Phys. **71**, 167 (1972); M. S. P. Eastham and H. Kalf, *Schrödinger-Type Operators with Continuous Spectra* (Pitman, Boston, 1982).
[62] O. Olendski and L. Mikhailovska, Phys. Rev. B **72**, 235314 (2005).
[63] J. Dittrich and J. Kříž, J. Phys. A **35**, L269 (2002).
[64] O. Olendski and L. Mikhailovska, Phys. Rev. E **67**, 056625 (2003).
[65] D. Krejčiřík and J. Kříž, Publ. Res. Inst. Math. Sci. **41**, 757 (2005); D. Krejčiřík, ESAIM: COCV **15**, 555 (2009).
[66] E. R. Johnson, M. Levitin, and L. Parnovski, SIAM J. Math. Anal. **37**, 1465 (2006).
[67] O. Olendski and L. Mikhailovska, Phys. Rev. B **77**, 174405 (2008).
[68] E. S. Trifanova, Pis'ma Zh. Tekh. Fiz. **35** (4), 60 (2009) [Tech. Phys. Lett. **35**, 180 (2009)].
[69] P. Freitas and D. Krejčiřík, Math. Phys., Anal. Geom. **9**, 335 (2006).
[70] A. G. Gurevich, *Ferrites at Microwave Frequencies* (Consultants Bureau, New York, 1963).
[71] A. J. Baden Fuller, *Ferrites at Microwave Frequencies* (Peter Peregrinus, London, UK, 1987).
[72] E. N. Bulgakov, P. Exner, K. N. Pichugin, and A. F. Sadreev, Phys. Rev. B **66**, 155109 (2002).
[73] F. E. Grigor'yan, Akust. Zh. **14**, 376 (1968) [Sov. Phys. Acoust. **14**, 315 (1969)]; Akust. Zh. **16**, 229 (1970) [Sov. Phys. Acoust. **16**, 192 (1970)].
[74] S. H. Ko and L. T. Ho, J. Sound Vib. **53**, 189 (1977); S.-H. Ko, *ibid.* **66**, 165 (1979).
[75] W. Rostafinski, J. Acoust. Soc. Am. **71**, 36 (1982).
[76] S. Félix and V. Pagneux, J. Acoust. Soc. Am. **116**, 1921 (2004).
[77] W. P. Bi, V. Pagneux, D. Lafarge, and Y. Aurégan, J. Sound Vib. **289**, 1091 (2006).
[78] A. F. Slachmuylders, B. Partoens, and F. M. Peeters, Phys. Rev. B **71**, 245405 (2005).
[79] *Handbook of Mathematical Functions*, edited by M. Abramowitz and I. A. Stegun (Dover, New York, 1964).
[80] E. Bahar, IEEE Trans. Microwave Theory Tech. **17**, 210 (1969).
[81] W. C. Osborne, J. Sound Vib. **45**, 39 (1976).
[82] J. A. Cochran, J. Soc. Ind. Appl. Math. **12**, 580 (1964).
[83] V. V. Nesvizhevsky, A. K. Petukhov, K. V. Protasov, and A. Y. Voronin, Phys. Rev. A **78**, 033616 (2008).
[84] R. Landauer, IBM J. Res. Dev. **1**, 223 (1957); **32**, 306 (1988); Philos. Mag. **21**, 863 (1970).
[85] I. S. Gradshteyn and I. M. Ryzhik, *Table of Integrals, Series, and Products* (Academic, New York, 2000).
[86] A. P. Prudnikov, Yu. A. Brychkov, and O. I. Marichev, *Inte-*

grals and Series (Gordon and Breach Science Publishers, New York, 1986), Vols. 2 and 3.

[87] Yu. A. Brychkov, *Special Functions: Derivatives, Integrals, Series and Other Formulas* (Chapman, Boca Raton, 2008).

[88] K. Lin and R. L. Jaffe, Phys. Rev. B **54**, 5750 (1996).

[89] V. V. Moshchalkov, J. Supercond. Novel Magn. **19**, 409 (2006).

[90] P. S. Deo, V. A. Schweigert, F. M. Peeters, and A. K. Geim, Phys. Rev. Lett. **79**, 4653 (1997).

[91] A. K. Geim, I. V. Grigorieva, S. V. Dubonos, J. G. S. Lok, J. C. Maan, A. E. Filippov, and F. M. Peeters, Nature (London) **390**, 259 (1997).

[92] M. Morelle, D. S. Golubović, and V. V. Moshchalkov, Phys. Rev. B **70**, 144528 (2004); L. F. Chibotaru, A. Ceulemans, M. Morelle, G. Teniers, C. Carballeira, and V. V. Moshchalkov, J. Math. Phys. **46**, 095108 (2005).

[93] B. Z. Katsenelenbaum, *High-Frequency Electrodynamics* (Wiley, Weinheim, Germany, 2006).